Probability Distribution of Multiple Scattered Light Measured in Total Transmission

Johannes F. de Boer,[1] M. C. W. van Rossum,[1] Meint P. van Albada,[2] Th. M. Nieuwenhuizen,[1] and Ad Lagendijk[1,2]
[1]*van der Waals-Zeeman Laboratorium, Universiteit van Amsterdam, Valckenierstraat 65, 1018 XE Amsterdam, The Netherlands*
[2]*FOM-Institute for Atomic and Molecular Physics, Kruislaan 407, 1089 SJ Amsterdam, The Netherlands*
(Received 19 April 1994)

We report the first measurement of the distribution function of the fluctuations on the total transmission of multiple scattered light. The shape of the distribution is predominantly Gaussian. A non-Gaussian contribution to the distribution function is found, caused by correlation in the cubed intensity. The scattering diagrams responsible for this new correlation are calculated without free parameters, and a good agreement is found between experiment and theory.

PACS numbers: 42.25.Bs, 72.15.−v, 78.20.Dj

Multiple scattering of waves in disordered systems is a field of wide interest and is studied with light, sound waves, and electrons. Interference between waves in the multiple scattering regime can play an important role and leads to a variety of effects such as enhanced backscattering [1], short-range and long-range correlation in the intensity fluctuations [2–6], universal conductance fluctuations (UCF) [7], and ultimately to Anderson localization.

Recently the full distribution function of these fluctuations has received a lot of attention [8–11]. Experiments with light form an excellent way to measure these fluctuations. Genack and Garcia [8] showed experimentally that in the multiple scattering regime the intensity statistics of the speckle changes from Rayleigh for small intensity speckles to a stretched exponential for large intensity speckles. This was confirmed theoretically by Kogan *et al.* [9], who also predicted a Gaussian distribution for the fluctuations on the total transmission of light. In computer simulations Edrei, Kaveh, and Shapiro [10] found a Gaussian distribution of the total transmission in two dimensions in the diffusive regime, which changed to a log-normal distribution for increasing disorder. The same behavior is predicted for the conductance of electronic systems as one approaches the Anderson transition [11].

In this Letter we present the experimental distribution function of the fluctuating light intensity in total transmission through a disordered slab. The data show a distribution that is almost Gaussian but contains a small but significant non-Gaussian contribution due to the presence of a third cumulant. It expresses a correlation in the cubed total transmission, which is different from the well-established optical short-range and long-range correlations.

Let us first describe the different configurations to observe fluctuations with the help of the following model. The sample consists of a static arrangement of scatterers, with $L \gg \ell \gg \lambda$, L is the sample thickness, ℓ is the mean free path, and λ is the wavelength of the light. The random sample can be considered as a waveguide supporting N modes or channels, where the disorder couples all ingoing to all outgoing modes. The average transmission coefficient $\langle T_{ab}\rangle \sim \ell/NL$ gives the average fraction of the intensity that is coupled from incoming mode a into outgoing mode b. Angular brackets denote averaging over disorder. Varying the wavelength of the incoming light plays the role of changing the realization of the disorder, and the fluctuations are observed as a function of the wavelength. Fluctuations can be observed on the transmission (one-mode-in–one-mode-out), the total transmission (one-mode-in–all-modes-out), and the "conductance" (all-modes-in–all-modes-out).

The transmission coefficient T_{ab} follows initially an exponential (Rayleigh) distribution [12], while for large transmission coefficients a stretched exponential occurs [8,9]. The distribution has a relative variance $\langle \delta T_{ab}^2\rangle/\langle T_{ab}\rangle^2 \approx 1$, with $\delta T_{ab} = T_{ab} - \langle T_{ab}\rangle$.

The total transmission is obtained by summing over all outgoing modes, $T_a = \sum_b T_{ab} \sim \ell/L$. Naively one would expect for the distribution function $P(T_a)$ a convolution of N independent Rayleigh distributions which for large N becomes a Gaussian distribution with relative variance $1/N$. However, the interference between two light paths inside the sample correlates outgoing modes [13]. This results in an increase of the relative variance by a factor L/ℓ, and leads to [9,10]

$$P(T_a) \sim \exp\left|-\frac{1}{2}\frac{(T_a - \langle T_a\rangle)^2}{\langle \delta T_a^2\rangle}\right|, \tag{1}$$

with relative variance $\langle \delta T_a^2\rangle/\langle T_a\rangle^2 \sim L/N\ell$.

The conductance is given by $g \equiv \sum_{a,b} T_{ab} \sim N\ell/L$ with relative variance $\langle \delta g^2\rangle/\langle g\rangle^2 \sim \langle g\rangle^{-2}$ [13,14]. In electronic systems Altshuler, Kravtsov, and Lerner [11] predicted a distribution of the conductance $P(g)$, with the nth normalized cumulant $\langle\langle g^n\rangle\rangle$ (i.e., the nth cumulant over $\langle g\rangle^n$) proportional to $\langle g\rangle^{2-2n}$. In the metallic regime (i.e., for large values of the average conductance) the distribution is predominantly Gaussian. To our knowledge, neither the measurement of the conductance distribution in the metallic regime nor of the total transmission distribution of optical systems has been reported.

We measured the fluctuations in the total transmission using the setup described in detail in Ref. [17]. The samples consisted of TiO_2 particles in air, with an absorption length $\ell_a \simeq 70\ \mu$m. The mean free path ℓ for all samples was $\simeq 0.8\ \mu$m. In the experiment the

0031-9007/94/73(19)/2567(4)$06.00

thickness of the samples and the width of the incident Gaussian beam were varied to measure the fluctuations for different values of g. Table I lists the thickness of the samples, the width of the beam, and the number of scans over which was averaged to obtain the probability distribution and the second and third cumulant.

Figure 1 shows the measured distribution function summed over all samples and beamwidths to improve the statistics. Before summing the probability distributions of the scans the second cumulant of each scan was scaled to unity (FWHM is $2\sqrt{2\ln 2}$). The upper part of Fig. 1 shows the full distribution function, the solid line is the Gaussian of Eq. (1). The lower half of the graph shows the difference between the measured distribution and the Gaussian distribution, smoothed over half a unit of the x axis. The predicted effect of a third cumulant is shown by the solid line. Scaling the second cumulant to unity fixes its zero crossings, its vertical scale relates to the magnitude of the third cumulant. The shape of the $\delta P(T_a)$ curve clearly demonstrates the presence of a third cumulant in the measured distribution.

So the distribution is characterized by a second cumulant and a small but significant third cumulant, both of which need to be calculated. The normalized second cumulant is

$$\langle\langle T_a^2\rangle\rangle \equiv \frac{\langle T_a^2\rangle - \langle T_a\rangle^2}{\langle T_a\rangle^2} \sim \frac{L}{N\ell}. \qquad (2)$$

Double brackets define normalized cumulants. The second moment of the intensity distribution contains a disconnected [Fig. 2(a)] and a connected part [Fig. 2(b)]. The connected part [Fig. 2(b)] contains the interference between two diffusons (at a Hikami vertex [15]) and is proportional to $L/N\ell$ [13], which is the leading contribution to the second cumulant. The contribution to the second cumulant of the disconnected part is proportional to $1/N$, the naively predicted variance on the total transmission.

The diagrams contributing to the third moment are given in Fig. 3. From their structure the contribution to the third cumulant of the diagrams in Figs. 3(a), 3(b), and 3(c) are seen to be proportional to, respectively, $1/N^2$, $L/N^2\ell$, and $L^2/N^2\ell^2$. The leading contribution to the third cumulant of the intensity distribution comes from the connected diagrams [Fig. 3(c)]. The factor $L^2/N^2\ell^2$ can be interpreted as the probability that three light paths will interfere twice, just as $L/N\ell$ gives the probability that two light paths will interfere once. As an important result a quadratic relation between the second and the third normalized cumulant is found: $\langle\langle T_a^3\rangle\rangle \propto \langle\langle T_a^2\rangle\rangle^2$.

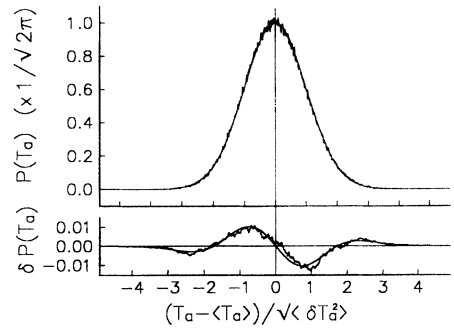

FIG. 1. Probability distribution of the fluctuations in total transmission, summed over all samples after scaling the second cumulant to unity. Upper graph: Full distribution. The solid line is a Gaussian. Lower graph presents the difference between the measured distribution and the Gaussian. The solid line shows the contribution expected from a third cumulant.

To verify this predicted quadratic relation between the second and third cumulant, we plot in Fig. 4 the third cumulant versus the second cumulant for each value of the conductance, i.e., for each value of the sample thickness and beam diameter (the mean free path was the same for all samples). The error bars were obtained from the variance in the second and third cumulant within a set of scans with the same sample thickness and beamwidth. The second and third cumulant are averaged over sets of 16, 32, 48, or 64 scans. The resulting values and their

TABLE I. Sample parameters in the experiment.

Sample thickness L (μm)	Beamwidth ρ_0 (μm)	Number of scans	Second cumulant ($\times 10^{-4}$)	Third cumulant ($\times 10^{-7}$)	Number of modes N^*
30	77	16	0.36 ± 0.01	0.014 ± 0.035	193 000
12	26	32	0.97 ± 0.03	−0.03 ± 0.25	23 300
22	32	48	1.24 ± 0.04	0.68 ± 0.28	43 500
30	33	16	1.57 ± 0.04	1.30 ± 0.46	57 300
53	35	32	1.80 ± 0.03	0.91 ± 0.53	112 000
30	26	32	1.90 ± 0.03	0.92 ± 0.56	45 000
45	33	32	1.90 ± 0.05	1.33 ± 0.43	87 600
53	26	32	2.18 ± 0.03	1.77 ± 0.59	94 500
170	27	32	2.69 ± 0.06	2.02 ± 0.82	632 000
78	28	64	2.74 ± 0.03	2.43 ± 0.62	177 000
30	17	16	4.82 ± 0.10	9.1 ± 3.3	33 000
30	10	32	8.01 ± 0.36	5.3 ± 6.4	26 700

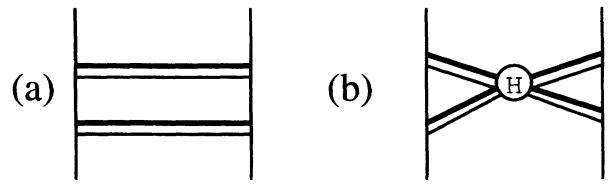

FIG. 2. Diagrams contributing to the second moment of the fluctuations on the total transmission. Diffusons (diffuse propagating intensities) are depicted by close parallel lines. (a) Two disconnected diffusons. (b) Two diffusons interfering inside the sample. This is the leading contribution to the second cumulant.

standard error are given in Table I. The expected standard error of a third cumulant due to finite sampling can be estimated to be $(15/N_p)^{1/2}\langle\langle T_a^2\rangle\rangle^{3/2}$, with N_p the number of points in a scan (1024) times the number of scans. The experimental error bars on the third cumulant are in good agreement with the expected magnitude of the standard error. The solid line is a weighted nonlinear least squares fit of $\langle\langle T_a^3\rangle\rangle = \alpha\langle\langle T_a^2\rangle\rangle^\beta$ to the data. The minimum of the χ^2 merit function is 9.0 for $\alpha = 0.7$ and $\beta = 1.83$, and the 68% confidence region is given by the contour $\chi^2 = 11.5$, shown in the inset in Fig. 4. This yields a prefactor $\alpha = 0.7^{+6.0}_{-0.7}$ and a power $\beta = 1.83 \pm 0.26$, which is in good agreement with the predicted quadratic relation. The probability to have measured our data set given a linear or a quadratic parent function is, respectively, 0.035% and 53%. A fit of the quadratic behavior ($\beta = 2$) yields a prefactor $\alpha = 2.9 \pm 0.6$.

To determine the prefactor of the quadratic relation between the second and the third cumulant an explicit calculation of the diagrams in Figs. 2(b) and 3(c) has to be done that includes the incident Gaussian beam profile, $I_{\rm inc}(\mathbf{r}_\perp) \sim \exp(-2\mathbf{r}_\perp^2/\rho_0^2)$. Since the number of modes in transmission and reflection is loosely defined for a Gaussian intensity profile on a transverse infinite slab, a definition of N is used where $1/N$ is equal to the contribution of the diagram in Fig. 2(a) to the second cumulant. Taking into account the diffuse broadening of the beam inside the sample this leads to

$$N \equiv 2\frac{k^2 I^2(q=0)}{\int_0^\infty 2qI(q)I(-q)dq}, \tag{3}$$

with k the wave vector of the light and $I(q)$ the Fourier transform of the intensity profile at the exit interface of the sample. The factor 2 distinguishes the vector wave ($2 = 2$) from the scalar wave ($2 = 1$) results [17]. In the limit $\rho_0 \gg L$ the number of modes N is not influenced by the diffuse broadening of the incident profile, $N = 2k^2\rho_0^2/4$. In this limit the conductance $g = 4N\ell/3L$ is now given by

$$g = \frac{2k^2\rho_0^2\ell}{3L}. \tag{4}$$

The results for the second cumulant [Fig. 2(b)] are well known [13,14,16] and give ($\rho_0 \gg L$)

$$\langle\langle T_a^2\rangle\rangle = \frac{2L}{2k^2\rho_0^2\ell} = \frac{2}{3}g^{-1}. \tag{5}$$

In Fig. 3(c) we present the third cumulant, the first diagram contains two Hikami four-point vertices, the second a six-point vertex. In the calculation the six-point vertex is found to cancel against the extra contribution of the first diagram that arises when the distance between the two Hikami vertices is of the order of one mean free path. The third cumulant depends in a nontrivial manner on the beam profile. For the incident Gaussian profile we find ($\rho_0 \gg L$)

$$\langle\langle T_a^3\rangle\rangle = \frac{64L^2}{2^2\,5k^4\rho_0^4\ell^2} = \frac{64}{45}g^{-2}. \tag{6}$$

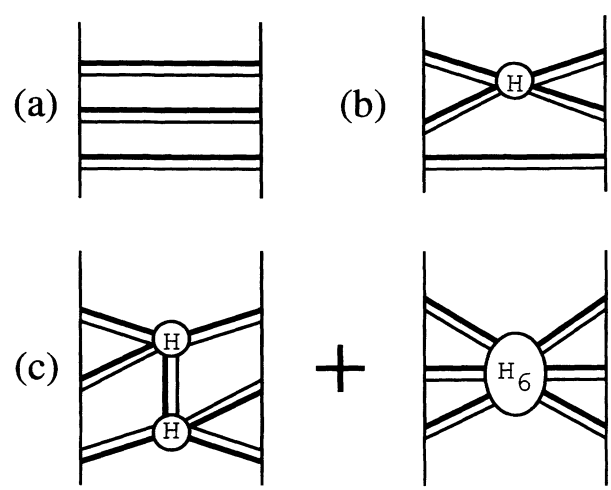

FIG. 3. The diagrams contributing to the third moment of the fluctuations on the total transmission. (a) Three disconnected diffusons. (b) Two interfering diffusons and a disconnected diffuson. (c) Three interfering diffusons, the first through two Hikami vertices, the second through a six-point vertex. The latter are the leading contributions to the third cumulant.

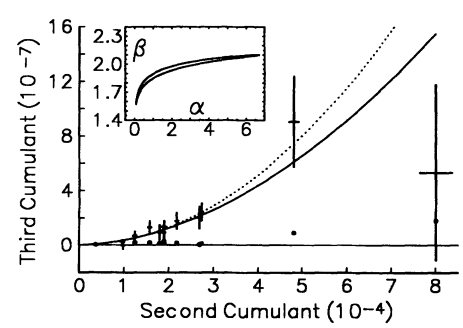

FIG. 4. The third cumulant as a function of the second cumulant of the intensity distribution. Solid line is weighted least squares fit to the data of $\langle\langle T_a^3\rangle\rangle = \alpha\langle\langle T_a^2\rangle\rangle^\beta$. The inset shows the 68% confidence region of the fit parameters α and β, yielding $\alpha = 0.7^{+6.0}_{-0.7}$, $\beta = 1.83 \pm 0.26$. Dashed line is theoretical prediction $\langle\langle T_a^3\rangle\rangle = 3.2\langle\langle T_a^2\rangle\rangle^2$. Dots show the upper bound of the contribution of the mundane diagram in Fig. 3(b) to the third cumulant.

(For a square profile the result would be $16/15g^2$.) This gives the following simple relation between the second and third cumulant,

$$\langle\langle T_a^3\rangle\rangle = \frac{16}{5}\langle\langle T_a^2\rangle\rangle^2. \tag{7}$$

The experimentally observed prefactor of 2.9 ± 0.6 is in good agreement with the theoretical value of 16/5.

Let us now estimate higher order effects and the influence of the experimental beamwidth $\rho_0 \sim L$. The contribution to the second cumulant of the diagram in Fig. 2(a) yielded $1/N$ [Eq. (3)] and can be neglected. The leading correction to Eq. (6) comes from the diagram in Fig. 3(b), which gives $\Delta\langle\langle T_a^3\rangle\rangle \leq 6\langle\langle T_a^2\rangle\rangle/N^*$. The factor of 6 is of combinatorial origin and the effective number of modes N^* differs from N because it is the product of a single diffuson with the second cumulant diagram. N^* is given by

$$N^* \simeq 2\frac{k^2 I(q=0)}{\int_0^\infty 2qI(q)dq}. \tag{8}$$

Table I gives the number of modes N^* for each sample and each incident beamwidth ($2 = 2$). The resulting upper bound of the magnitude of the diagram in Fig. 3(b) is shown in Fig. 4 by the dots.

The magnitudes of the second cumulant as calculated with the experimental parameters as input are larger than the measured values by maximally 25%. This difference was addressed in Ref. [17], where it was shown to be caused by the finite range over which the wavelength was varied in the experiment. For the same reason the experimental values of the third cumulant are also lower than predicted. By plotting the second versus the third cumulant (Fig. 4) the effects of the finite scan length largely cancel, as do effects of inaccuracies in the exact beamwidth, mean free path, and sample thickness.

The influence of the beamwidth was numerically evaluated for the diagrams of Figs. 2(b) and 3(c). The resulting relation between the second and third cumulant remained quadratic, only the prefactor of 16/5 was reduced by at most 14% for the smallest value of ρ_0/L. If this reduction were included in the theory, it would make the agreement with the observed prefactor even better.

In conclusion, we showed experimentally that the probability distribution of the fluctuations in total transmission is predominantly Gaussian. The data clearly demonstrate a skewness of the probability distribution, caused by correlation in the cubed intensity. These correlations were calculated within a diagrammatic approach, and a good agreement is found between the experiment and the theory. The skewness in the experimental distribution is the first sign of a possible change from a Gaussian to a lognormal distribution, as is predicted to occur for the electronic conductance fluctuations [11].

The authors would like to thank E. Kogan and R. Sprik for helpful discussions. This work was supported in part by the Stichting voor Fundamenteel Onderzoek der Materie (FOM), which is a part of the Nederlandse Organisatie voor Wetenschappelijk Onderzoek. The research of Th. M. N. was supported by the Koninklijke Nederlandse Academie voor Wetenschappen (KNAW).

[1] M. P. van Albada and A. Lagendijk, Phys. Rev. Lett. **55**, 2692 (1985); P. E. Wolf and G. Maret, Phys. Rev. Lett. **55**, 2696 (1985). For recent reviews, see *Classical Wave Localization*, edited by P. Sheng (World Scientific, Singapore, 1990); *Photonic Band Gaps and Localization*, edited by C. M. Soukoulis NATO ASI Ser. B Vol. 308 (Plenum Press, New York and London, 1993).
[2] A. Z. Genack, Phys. Rev. Lett. **58**, 2043 (1987).
[3] I. Freund, M. Rosenbluh, and S. Feng, Phys. Rev. Lett. **61**, 2328 (1988).
[4] N. Garcia and A. Z. Genack, Phys. Rev. Lett. **63**, 1678 (1989).
[5] A. Z. Genack and J. M. Drake, Europhys. Lett. **11**, 331 (1990).
[6] M. P. van Albada, J. F. de Boer, and A. Lagendijk, Phys. Rev. Lett. **64**, 2787 (1990).
[7] C. P. Umbach, S. Washburn, R. B. Laibowitz, and R. A. Webb, Phys. Rev. B **30**, 4048 (1984).
[8] A. Z. Genack and N. Garcia, Europhys. Lett. **21**, 753 (1993).
[9] E. Kogan, M. Kaveh, R. Baumgartner, and R. Berkovits, Phys. Rev. B **48**, 9404 (1993).
[10] I. Edrei, M. Kaveh, and B. Shapiro, Phys. Rev. Lett. **62**, 2120 (1989).
[11] B. L. Altshuler, V. E. Kravtsov, and I. V. Lerner, in *Mesoscopic Phenomena in Solids*, edited by B. L. Altshuler, P. A. Lee, and R. A. Webb (North-Holland, Amsterdam, 1991).
[12] B. Shapiro, Phys. Rev. Lett. **57**, 2168 (1986).
[13] M. J. Stephen and G. Cwilich, Phys. Rev. Lett. **59**, 285 (1987).
[14] S. Feng, C. Kane, P. A. Lee, and A. D. Stone, Phys. Rev. Lett. **61**, 834 (1988).
[15] S. Hikami, Phys. Rev. B **24**, 2671 (1981).
[16] M. C. W. van Rossum and Th. M. Nieuwenhuizen, Phys. Lett. A **177**, 452 (1993).
[17] J. F. de Boer, M. P. van Albada, and A. Lagendijk, Phys. Rev. B **45**, 658 (1992).